

2

THE DEBORA DATABASE

Contents

2.1	Introduction	8
2.2	Simulating PWR water using R12	8
2.2.1	Conservation of the Phase Density Ratio	9
2.2.2	Conservation of the Weber Number	9
2.2.3	Conservation of the Boiling Number	10
2.2.4	Conservation of the Inlet Thermodynamic Quality	11
2.2.5	Same Geometry	11
2.2.6	Transposition ranges	11
2.3	Description of the Test Section	11
2.3.1	Geometrical Description	11
2.3.2	Measurement Instrumentation	12
2.4	Measurements Campaigns and Results	14
2.4.1	Cases Nomenclature and Test Series	14
2.4.2	Verification of Control Parameters Coherency	15
2.4.3	Qualitative Analysis of the Experimental Results	16
2.5	Further Verifications	21
2.5.1	Reconstruction of the Applied Heat Flux	21
2.5.2	Verification of Wall Temperature Measurements	23
2.6	Conclusions	25

2.1 INTRODUCTION

The validation of any existing modeling of multiphase flows must rely on extensive databases from experimental investigations in operating conditions that are representative of industrial configurations in PWR. This naturally lead to an important demand for measurements of local phase-related properties of vertical pressurized subcooled boiling flows.

To meet this need, CEA and EDF built a test facility called DEBORA in the 1990's. Its goal was to establish a consistent database of local measurements of the flow structure for vertical subcooled boiling freon Refrigerant 12 (R12) from the Onset of Nucleate Boiling to the Boiling Crisis.

In this chapter, we will describe the test section and analyze the available results from past measurements campaigns.

2.2 SIMULATING PWR WATER USING R12

The choice of using R12 as the working fluid in the DEBORA loop emerged from the interesting properties that boiling freon presents when compared to the highly pressurized water in PWR cores. Indeed, the conditions for which the Boiling Crisis must be studied for water in PWR are:

- Pressure P between 100 and 180 bar ;
- Inlet liquid mass flux G between 1000 and 5000 $\text{kg/m}^2/\text{s}$;

- Wall heat flux ϕ_w between 0.5 and 6 MW/m² ;
- Inlet thermodynamic flow quality $x_{eq,in}$ between -0.4 and 0.4.

In those ranges, sensors dedicated to local measurements are not suited to sustain such conditions.

The experimental strategy is then to "simulate" the aimed industrial conditions using a different fluid. It has to present thermophysical properties that allow to reproduce non-dimensional numbers of the industrial flow using less constraining operating conditions.

This explains the choice of R12 as it permits to transpose relevant parameters for PWR as detailed below.

2.2.1 Conservation of the Phase Density Ratio

Freon 12 can reach the same density ratio as water in PWR using limited pressurized conditions no larger than 30 bars. It is an important parameter to mimic the behavior of the boiling two-phase flow since it has a strong influence over the bubble size for example [32].

$$\left(\frac{\rho_{V,sat}}{\rho_{L,sat}}\right)_{P_1}^{water} = \left(\frac{\rho_{V,sat}}{\rho_{L,sat}}\right)_{P_2}^{R12} \quad (2.1)$$

with $P_2 < P_1$.

The evolution of the density ratio of water and R12 with pressure are shown on Figure 2.1.

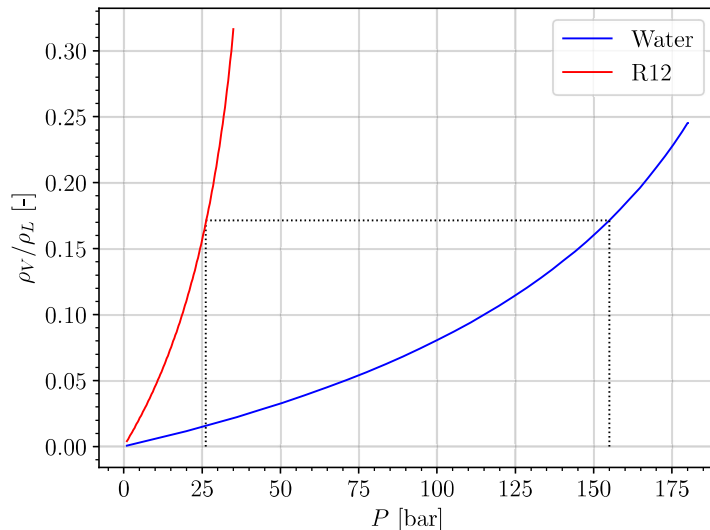


Figure 2.1: Density ratio of pressurized R12 and water

For instance, we can see that R12 at approximatively 26 bar ($T_{sat} \approx 86.8^\circ\text{C}$) has the same density ratio as water at 155 bar ($T_{sat} \approx 344.8^\circ\text{C}$).

Note : This tranposition criteria thus scales the operating pressure P of the experiment.

2.2.2 Conservation of the Weber Number

The Weber number is also similar to those encountered in PWR.

$$We = \frac{G^2 R}{\rho_L \sigma} \quad (2.2)$$

This number characterizes physical phenomena such as bubble break-up or deformation under the influence of the liquid inertia.

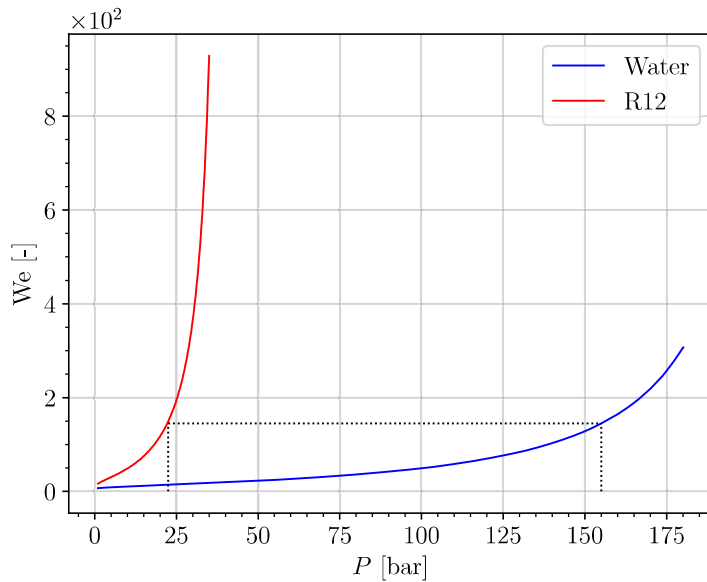


Figure 2.2: Weber number for R12 and water at $G = 2000 \text{ kg/m}^2/\text{s}$ and $R = 0.1 \text{ mm}$

Similar to the phase density ratio, Figure 2.2 shows that Weber number equivalent to water at 155 bar can be reached with R12 around 23 bar.

Note : For a same value of R , this transposition scales the inlet liquid mass flux G .

2.2.3 Conservation of the Boiling Number

The boiling number is defined as:

$$\text{Bo} = \frac{\phi_w}{Gh_{LV}} \quad (2.3)$$

It represents the comparison between the vapor mass flux ϕ_w/h_{LV} if all the heat flux contributes to phase change versus the inlet liquid mass flux. Thus, its value can be associated to the boiling and two-phase flow regime.

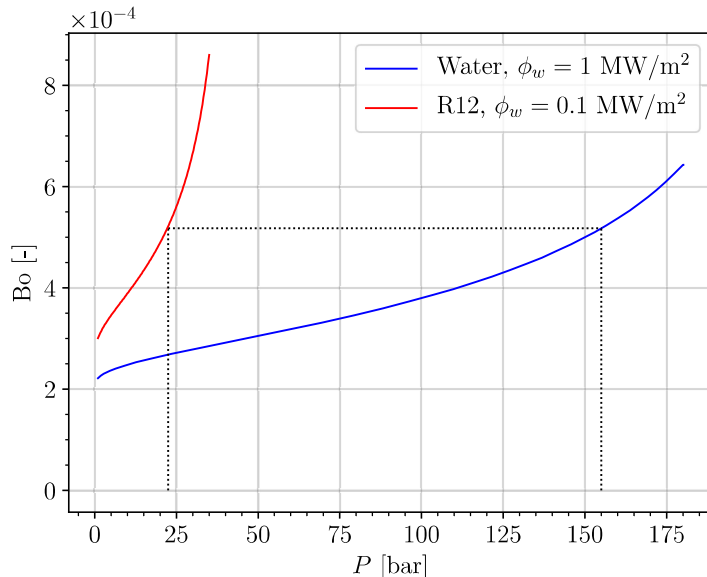


Figure 2.3: Boiling number for R12 and water at $G = 2000 \text{ kg/m}^2/\text{s}$

Figure 2.3 shows that Boiling number values similar to PWR can be reproduced using R12 with wall heat fluxes one order of magnitude lower and pressure around 23 bar.

Note : This transposition criteria scales the applied heat flux ϕ_w .

2.2.4 Conservation of the Inlet Thermodynamic Quality

Water in PWR being highly subcooled to avoid boiling, reproducing the inlet subcooling in the DEBORA experiment allows to mimic the early stages of boiling between the ONB and OSV. It allows to reproduce Boiling Crisis by Departure from Nucleate Boiling for low quality flows. This is achieved through the inlet thermodynamic quality:

$$x_{eq,in} = \frac{h_{L,in} - h_{L,sat}}{h_{LV}} \quad (2.4)$$

Note : This transposition is achieved by scaling the R12 inlet temperature.

2.2.5 Same Geometry

The last similarity achieved in the DEBORA experiment is related to the geometry. The heated length L_{ch} of the test section is similar to the height of a nuclear fuel assembly and the hydraulic diameter D_h is equal to that of a subchannel.

2.2.6 Transposition ranges

As a result of those conservation criteria, Table 2.1 sums up the transposition ranges for each parameters.

Fluid	Water	Freon R12
P [bar]	100 - 180	14 - 30
G [kg/m ² /s]	1000 - 5000	1000 - 5000
ϕ_w [MW/m ²]	0.5 - 6	0.05 - 0.65
$x_{eq,in}$ [-]	(-0.4) - (+0.4)	(-0.4) - (+0.4)
$\rho_{V,sat}/\rho_{L,sat}$ [-]	0.08 - 0.25	0.07 - 0.22
We [-]	49.5 - 307.1	69.1 - 365.8
$Bo \times 10^{-3}$ [-]	0.19 - 3.86	0.21 - 4.33

Table 2.1: Water R12 scaling, $R = 0.01\text{mm}$ for We

2.3 DESCRIPTION OF THE TEST SECTION

2.3.1 Geometrical Description

To apply the aforementioned transport criteria, four thermal-hydraulic control parameters are imposed in the test section:

- The outlet pressure P ;
- The inlet mass flow rate $G \times S_{in}$ with $S_{in} = \pi R^2 \approx 2.9 \times 10^{-4} \text{ m}^2$ the inlet area ;
- The inlet liquid temperature $T_{L,in}$;
- The electrical power transferred to the liquid $\phi_w \times S_{heat}$ with S_{heat} the heated area.

The test section is presented on Figure 2.4. It consists of an inconel tube with inner diameter $D_h = 19.2 \text{ mm}$, a 1 mm thickness and a heated length $L_{heat}=3.5 \text{ m}$. A detailed description of the whole experimental loop is given in Garnier *et al.* [21].

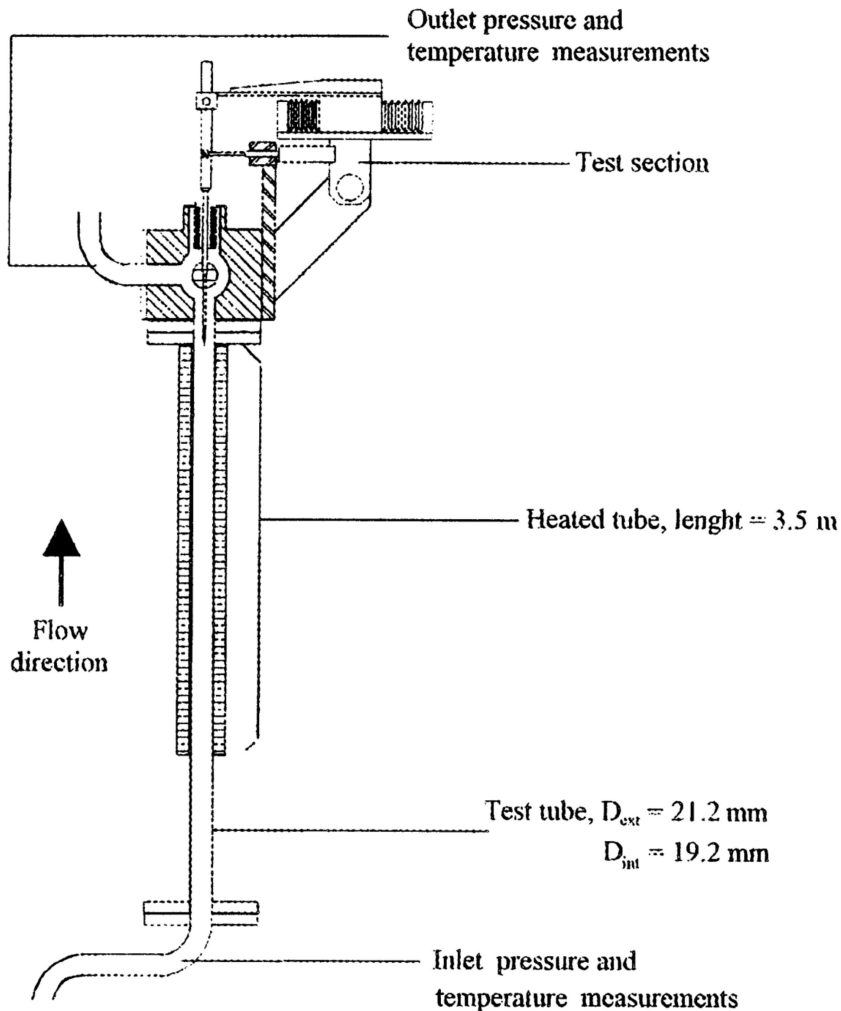


Figure 2.4: Sketch of the DEBORA test section. Adapted from [21].

2.3.2 Measurement Instrumentation

The control parameters are adjusted and measured using pressure, temperature, flow rate and power measurements. They are further detailed in Cubizolles [11].

The local measurements are conducted at the end of the heating length using a controllable probe that can cover the whole diameter of the test section with an accuracy of $10\mu\text{m}$. Only one diameter is covered since the chosen geometry induces an axisymmetry.

Three type of measurements have been conducted over different experimental campaigns.

2.3.2.1 Mono-Optical Probe Measurements

Optical probe measurement rely on the difference of optical refractive index between the liquid and vapor phase. Using an optical fiber in which light is emitted towards the probe tip allows to detect the actual phase flowing on the probe.

The resulting signal is called a Phase Indicator Function (PIF) which looks like to a square signal (Figure 2.5) that can be post-processed to identify the average time spent by the probe in each phase and then estimate their volume fraction *e. g.* the void fraction.

If the PIF is measured over a period T , the void fraction α at the measurement point x can be estimated by:

$$\alpha(x) = \nu(x) \bar{t_V} = \frac{1}{T} \sum t_V \quad (2.5)$$

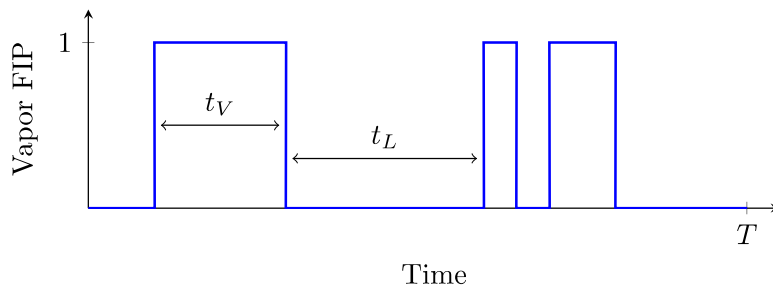


Figure 2.5: Example of Phase Indicator Function signal

where ν is called the interference frequency that represents the number of phase interface detection per second by the probe.

Note : This measurement technique was performed in the **measurement campaign C2900** where void fraction profiles at the outlet were obtained for various flow conditions.

2.3.2.2 Bi-Optical Probe Measurements

Using the technology of the optical phase detection, adding a second optical probe permits to measure more parameters of the two-phase flow. Indeed, the use of two probes placed close to each other with a small shift in the flow direction (Figure 2.6) allows to estimate the velocity of the interface between the two probes by measuring the time difference between the two PIF.

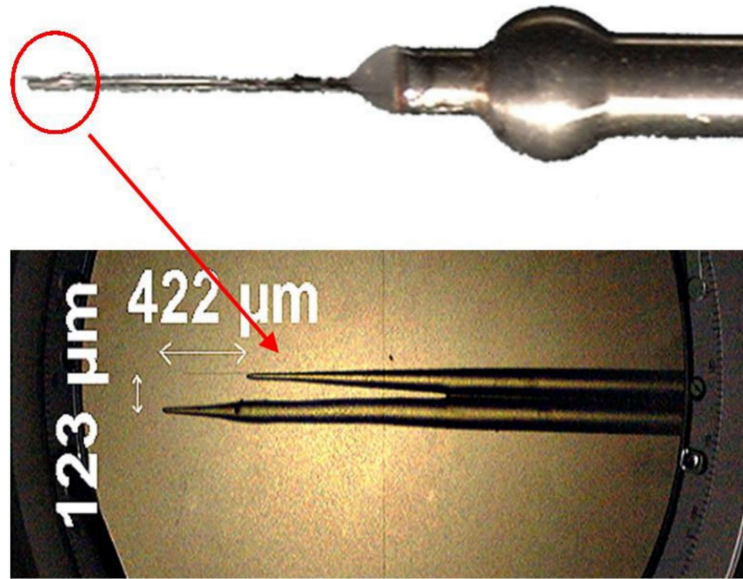


Figure 2.6: Picture of the bi-optical probe with a zoom over the two optical fibers. Reproduced from [24].

Considering the following assumptions:

- The flow is mainly one-directional in aligned with the probes ;
- The vapor phase is composed of spherical inclusions ;
- The velocity gradient and center density gradient are small along a bubble diameter length.

Then we can estimate:

- The vapor axial velocity $U_{V,z}$ that can be supposed equal to the measured interface velocity between the probes ;

- The interfacial area density a_i :

$$a_i = \frac{4\nu}{U_{V,z}} \quad (2.6)$$

- The bubble Sauter diameter:

$$D_V = \frac{6\alpha}{a_i} \quad (2.7)$$

Note : This measurement technique was performed in the **measurement campaign C3000**.

2.3.2.3 Thermocouples Measurements

Thermal measurements are conducted using chromel-alumel thermocouples. The liquid temperature is measured along the outlet diameter at the end of the heating length. Wall temperature measurements are conducted with 4 thermocouples placed at different heights (1.465 m, 2.465 m, 2.965 m, 3.485 m) on the outside of the tube.

Note : This measurement technique was performed in the **measurement campaign C800**.

2.4 MEASUREMENTS CAMPAIGNS AND RESULTS

2.4.1 Cases Nomenclature and Test Series

As mentioned before, three different campaigns have been performed:

- Campaign C2900 with solely void fraction measurements using mono-optical probe ;
- Campaign C3000 with void fraction, vapor velocity, bubble Sauter diameter and interfacial area density measurements using bi-optical probe ;
- Campaign C800 with liquid and wall temperature measurements using thermocouples.

Each measurement series is conducted under fixed outlet pressure, liquid mass flux and electrical power. Inlet temperature is then changed to cover different inlet quality. Experimental cases are named in the form **CccGgPppWwwTett** with **cc** the campaign number (29, 30 or 8), **g** the inlet mass velocity (G in $\text{t/m}^2/\text{s}$), **pp** the outlet pressure (P in bars), **ww** the total heat power applied (Φ_w in kW) and **tt** the inlet temperature ($T_{L,in}$ in K). For instance, the case named C30G2P26W16Te66 has been conducted with $P = 26.2$ bar, $G = 2049 \text{ kg/m}^2/\text{s}$, $\Phi_w = 15.6 \text{ kW} \equiv \phi_w = 73.89 \text{ kW/m}^2$ and $T_{L,in} = 66.59^\circ\text{C}$.

P	G	W16	W17	W23	W24	W25	W27	W29	W30	W31	W33	W34	W36	W38	W39	W40	W42	W44
14	2	○ ▽ △	△															
	4				○				▽	▽	▽	▽	▽	▽	▽	▽	▽	▽
	5							▽										
26	2	○ ▽ △								▽ △	▽	▽ △	▽	▽	▽ △	▽	▽	▽ △
	3			▽ △		▽ △		▽	▽ △	▽	▽ △	▽	▽	▽	▽ △	▽	▽	▽ △
	5	○			○													

P	G	W12	W14
30	1	▽	▽

Table 2.2: Test matrix of the DEBORA cases. ○: C800 - ▽: C2900 - △: C3000

If we want to obtain a full description of the two-phase flow from the DEBORA tests, we need to have measurements from campaigns C3000 and C800 (flow topology and thermal) with the same control parameters. Table 2.2 unfortunately shows that only very few test series between C3000 and C800 have common operating conditions, namely:

- Series 8G2P14W16 and 30G2P14W16 ;
- Series 8G2P26W16 and 30G2P26W16.

Other flow conditions have either been covered with thermal measurements or topology measurements but not both.

Remark : Cases from the campaign C2900 would only be relevant for void fraction profiles comparison. Estimations of the bubble diameter can not be achieved except if one assumes a velocity profile as suggested by Cubizolles [11] and re-used by Guéguel [24] who supposes:

$$U_{V,z}(r) \approx U_{M,z}(r) = 1.22 \frac{G}{\langle \rho_M \rangle_2} \left(\frac{R-r}{R} \right)^{1/7} \quad (2.8)$$

where $U_{M,z}$ is the mixture axial velocity, assuming a mechanical equilibrium between the phases.

For further studies, we will mainly focus on the G2P26W16 and G2P14W16 test series. Although we will mainly rely on the results from the C3000 campaign (where vapor velocity was actually measured) for flow topology qualification, we will evaluate the assumption of Eq. 2.8 with the C2900 measurements.

2.4.2 Verification of Control Parameters Coherency

For each case, the total heat input Φ_w is given along with the inlet mass flux G , inlet liquid temperature $T_{L,in}$ and outlet quality $x_{eq,out}$. To verify the consistency of those values, we can recalculate the outlet quality:

$$x_{eq,out,calc} = \frac{h_{M,out,calc} - h_{L,sat}}{h_{LV}} \quad (2.9)$$

with $h_{M,out,calc}$ the recalculated outlet mixture enthalpy:

$$h_{M,out,calc} = h_{in} + \frac{\Phi_w}{GS_{in}} = h_{in} + \frac{4\phi_w L_{heat}}{GD_h} \quad (2.10)$$

with h_{in} the inlet enthalpy calculated from the fluid properties using the inlet liquid temperature.

The difference between the given and recalculated outlet quality can also be converted to input power error by recalculating the heat needed to reach the given $x_{eq,out}$:

$$\Phi_{w,calc} = \frac{G\pi R^2}{\underbrace{[x_{eq,out}h_{LV} + h_{L,sat}] - h_{L,in}}_{h_{M,out}}} \quad (2.11)$$

Moreover, for a given set of experiments at the same P , G and Φ_w changing the inlet quality can be associated to moving the measurement diameter along the axial direction following the relationship:

$$x_{eq}(z) = x_{eq,in} + \frac{4\phi_w z}{GD_h h_{LV}} \quad (2.12)$$

Thus, taking the maximum inlet quality case $x_{eq,in,max}$ as a reference ($z = 3.5$ m), we can estimate the corresponding measurement height z_{eq} of each other cases if the inlet quality was $x_{eq,in,max}$.

We calculated the equivalent heights and outlet quality / power input errors for two series of the C3000 campaigns. Results are displayed on Tables ?? and ??.

As we can see, the given values of outlet quality for the 30G2P14W16 tests are coherent with the one-dimensional enthalpy balance with errors mostly less than 0.1% on the recalculated quality and less than

$T_{L,in}$ [K]	$x_{eq,in,calc}$ [-]	$x_{eq,out,calc}$ [-]	$x_{eq,out}$ [-]	z_{eq} [m]	$x_{eq,out}$ error [-]	Φ_w error [kW]
22.39	-0.317	-0.0821	-0.0832	1.075	0.114 %	-0.078
26.8	-0.28	-0.0422	-0.0431	1.653	0.089 %	-0.061
28.76	-0.263	-0.0267	-0.0273	1.896	0.056 %	-0.038
30.08	-0.252	-0.0152	-0.0157	2.065	0.05 %	-0.034
31.39	-0.241	-0.004	-0.0043	2.234	0.035 %	-0.023
38.95	-0.175	0.0674	0.0681	3.229	-0.072 %	0.049
39.96	-0.166	0.077	0.0776	3.357	-0.063 %	0.042
41.16	-0.155	0.0875	0.0882	3.509	-0.064 %	0.043

Table 2.3: Recalculated control parameters for the 30G2P14W16 cases. ($T_{sat} = 58.07^\circ\text{C}$)

$T_{L,in}$ [K]	$x_{eq,in,calc}$ [-]	$x_{eq,out,calc}$ [-]	$x_{eq,out}$ [-]	z_{eq} [m]	$x_{eq,out}$ error [-]	Φ_w error [kW]
58.57	-0.395	-0.0893	-0.0819	1.792	-0.747 %	0.381
60.54	-0.370	-0.0650	-0.0578	2.072	-0.722 %	0.369
62.54	-0.344	-0.0392	-0.0318	2.369	-0.741 %	0.378
64.6	-0.318	-0.0123	-0.0050	2.674	-0.736 %	0.376
66.59	-0.292	0.0140	0.0213	2.973	-0.728 %	0.371
68.57	-0.266	0.0402	0.0473	3.271	-0.716 %	0.365
70.59	-0.239	0.0670	0.0743	3.583	-0.723 %	0.369

Table 2.4: Recalculated control parameters for the 30G2P26W16 cases. ($T_{sat} = 86.81^\circ\text{C}$)

100 W on the recalculated power input. This naturally leads to an equivalent height very close to 3.5 m for the hottest case.

However, a more significant error is observed on the 30G2P26W16 cases where errors up to 0.75% on the outlet quality and close to 0.4 kW on the power input are found. Those values are significant especially for cases close to saturation where uncondensed vapor will start to appear in the bulk. Moreover, this results in an equivalent height 8.3 cm longer than the actually 3.5m heated length.

Since the inlet temperature, mass flux and power input are controlled parameters for each test, it is likely that the error may come from the given value of outlet quality $x_{eq,out}$ which is calculated and not imposed.

Note : Similar quality / input power errors were obtained on corresponding C29 and C8 campaigns:

- Negligible errors on for 29G2P14W16 and 8G2P14W16 cases ;
- Roughly 0.7 % outlet quality error and 0.3 to 0.4 kW power error for 29G2P26W16 and 8G2P26W16 cases.

2.4.3 Qualitative Analysis of the Experimental Results

On Figures 2.7, 2.8, 2.9 and 2.10 we respectively plot the experimental measurements of cases 29/30G2P26W16, 8G2P26W16, 29/30G2P14W16 and 8G2P14W16. The colorbar representing the outlet quality of each test is based on the computed value of $x_{eq,out}$ (Eq. 2.9).

2.4.3.1 G2P26W16 cases

Void fraction profiles obtained in for C2900 (single optical probe) and C3000 (bi-optical probe) cases are compared to verify the consistency of the measurements (Figure 2.7a). The two campaigns are in good agreement with each other, displaying a void fraction profile monotonously increasing with the outlet quality. The estimation of the vapor velocity by Eq. 2.8 for the C29 results is acceptable but presents

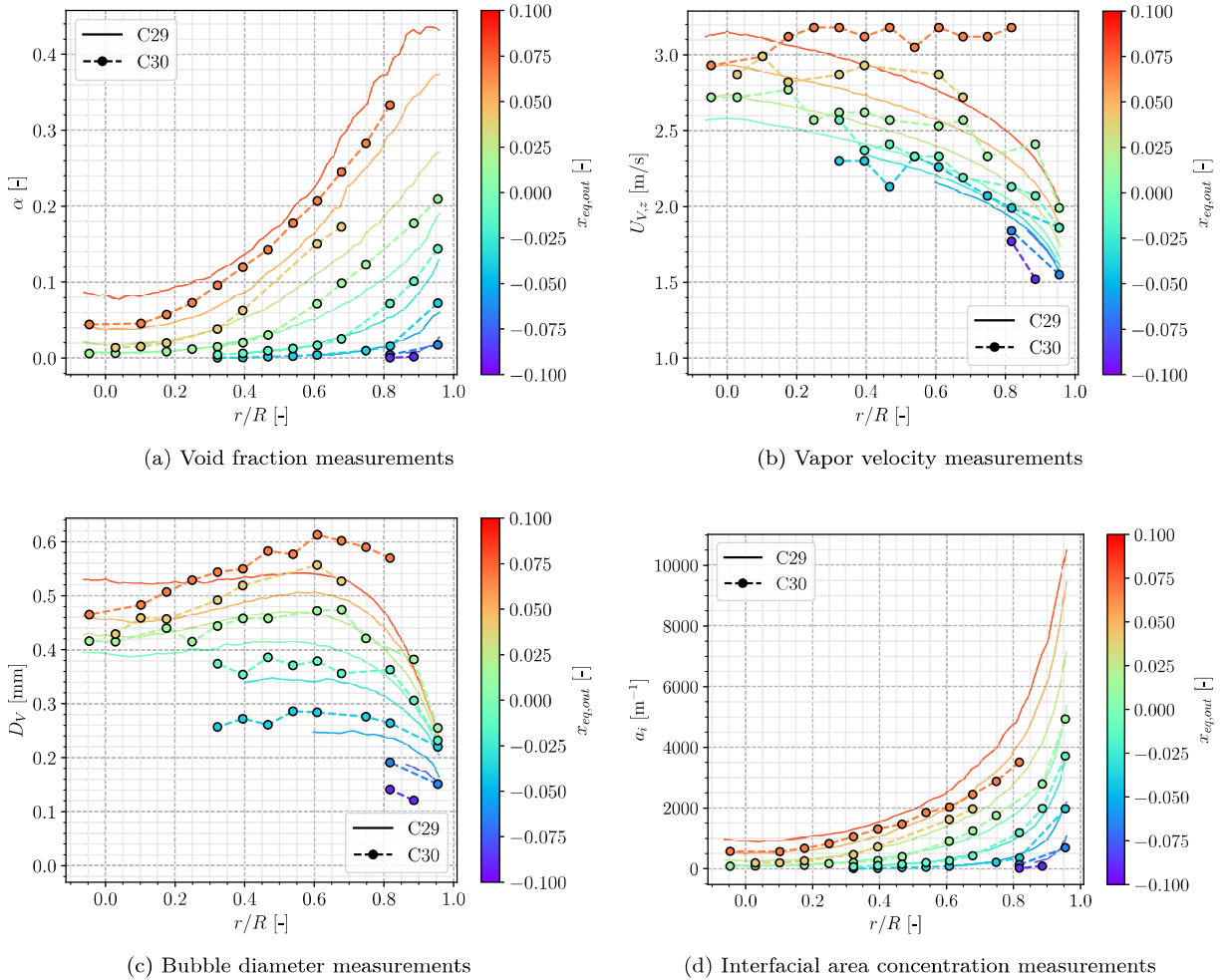


Figure 2.7: 30G2P26W16 and 29G2P26W16 results

an growing underestimation as the outlet title increases (Figure 2.7b). This results in bubble diameter underestimation close to the wall and consequently interfacial area overestimation.

We observe that the void fraction naturally increases with the outlet quality and that we reach net vapor generation with $\alpha(R = 0) > 0$ when $x_{eq,out} > 0$. Otherwise, vapor is not detected over the whole measurement section. Each case has its maximum void fraction near the wall with values up to approximately 40% when the outlet quality approaches 0.1.

The bubble diameter displays different behaviors (Figure 2.7c):

- It grows from the wall and reaches a maximum around $r/R \approx 0.6$, indicating bubble coalescence ;
- It stays nearly constant for negative outlet quality cases ;
- It decreases from $r/R = 0.6$ to $r/R = 0$ for saturated cases , indicating either bubble break-up or bulk condensation.

Remark : It seems that bubble diameter very close to the wall do not vary much between different cases, indicating that bubbles leave the wall at a nearly constant diameter over the different explored liquid temperatures ($D_V \approx 0.2$ mm).

Vapor velocity also increases with the outlet quality, with a nearly flat profile reached for saturated cases. The increase in vapor velocity may result of the larger bubble diameters which enhance the effect of buoyancy, acting as an accelerating term increasing the drift velocity.

Remark : Eq. 2.8 fails to predict this flattening of the vapor velocity on C2900 cases, which may indicate a change in the flow structure that can not be detected when assuming liquid-vapor mechanical equilibrium.

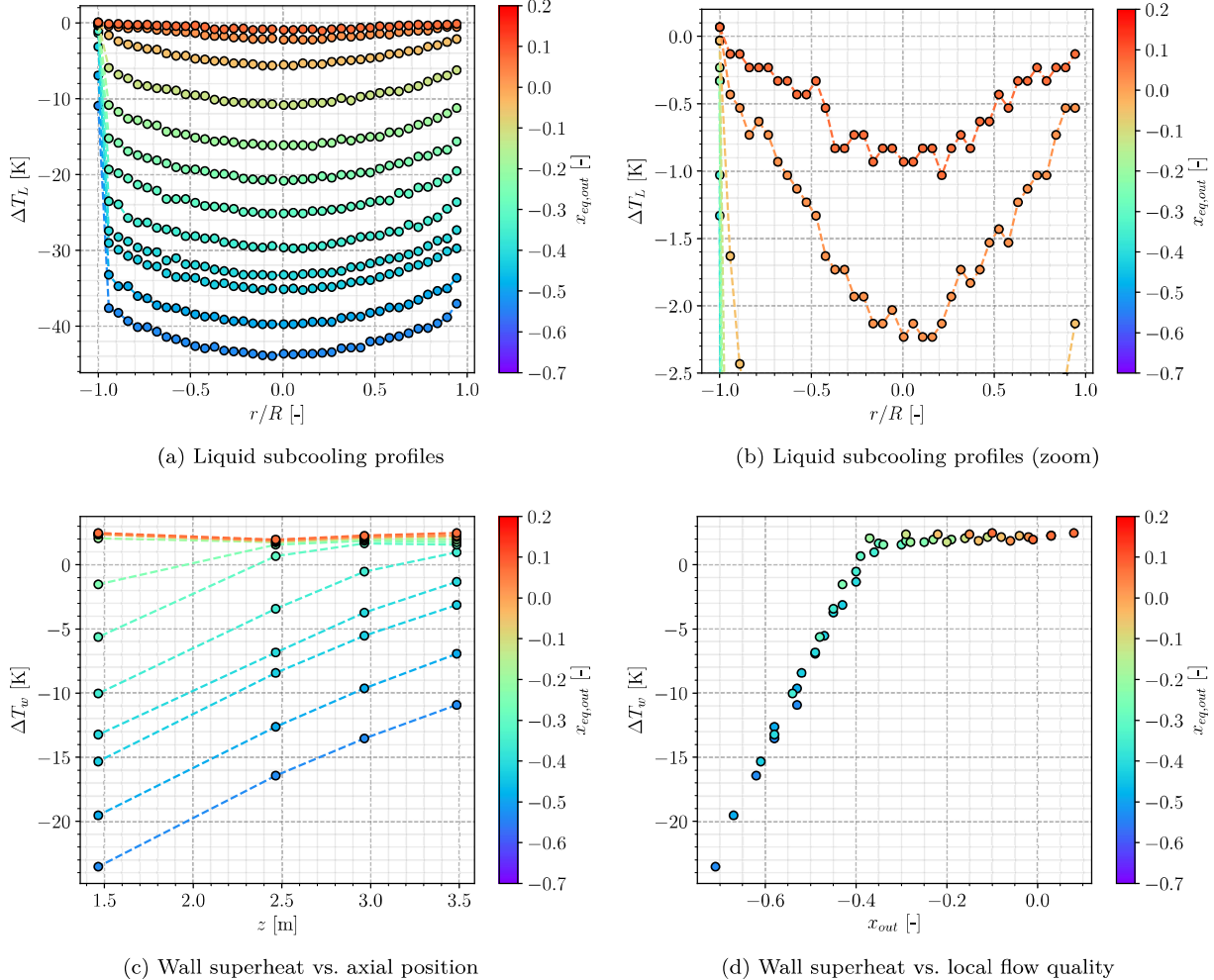


Figure 2.8: 8G2P26W16 results

Regarding the liquid temperature measurements (Figures 2.8a and 2.8b), we see that temperature profiles linearly rise with the inlet quality while presenting an unmodified parabolic shape. The only change appears when reaching significant superheated conditions ($x_{eq,out} \sim 0.1$) where the liquid temperature profile flattens over the test section.

Moreover, we observe that measurements very close to the wall present a very large temperature gradient even for low quality cases (temperature jump of nearly 30 degrees for coldest cases). This jump reduces as flow quality increases and reduces even more for boiling cases, indicating the well-known rise of the global heat transfer coefficient in boiling regime vs. single-phase convection regime.

We can also note that for the hottest case, the liquid becomes superheated near the wall ($\Delta T_L (\pm 1) \approx 0.1^\circ\text{C}$). The bulk is still slightly subcooled with $\Delta T_L (0) = -1^\circ\text{C}$

Remark : The liquid being subcooled in the bulk for superheated cases hints that the decrease in bubble diameter observed in Figure 2.7c for $r/R < 0.6$ may be associated to condensation.

Wall temperature measurements (Figures 2.8c) display linear growth for subcooled cases which is in agreement with traditional liquid convection problems. When reaching boiling, the wall superheat stabilizes at $\Delta T_w \approx 2^\circ\text{C}$. Rearranging the different wall temperature measurements versus the local flow quality

(Figure 2.8d) presents a coherent overlapping between cases with different inlet subcooling. This further validates the transposition of inlet quality into variation into an evolution of the measurement probe's axial position.

2.4.3.2 G2P14W16 cases

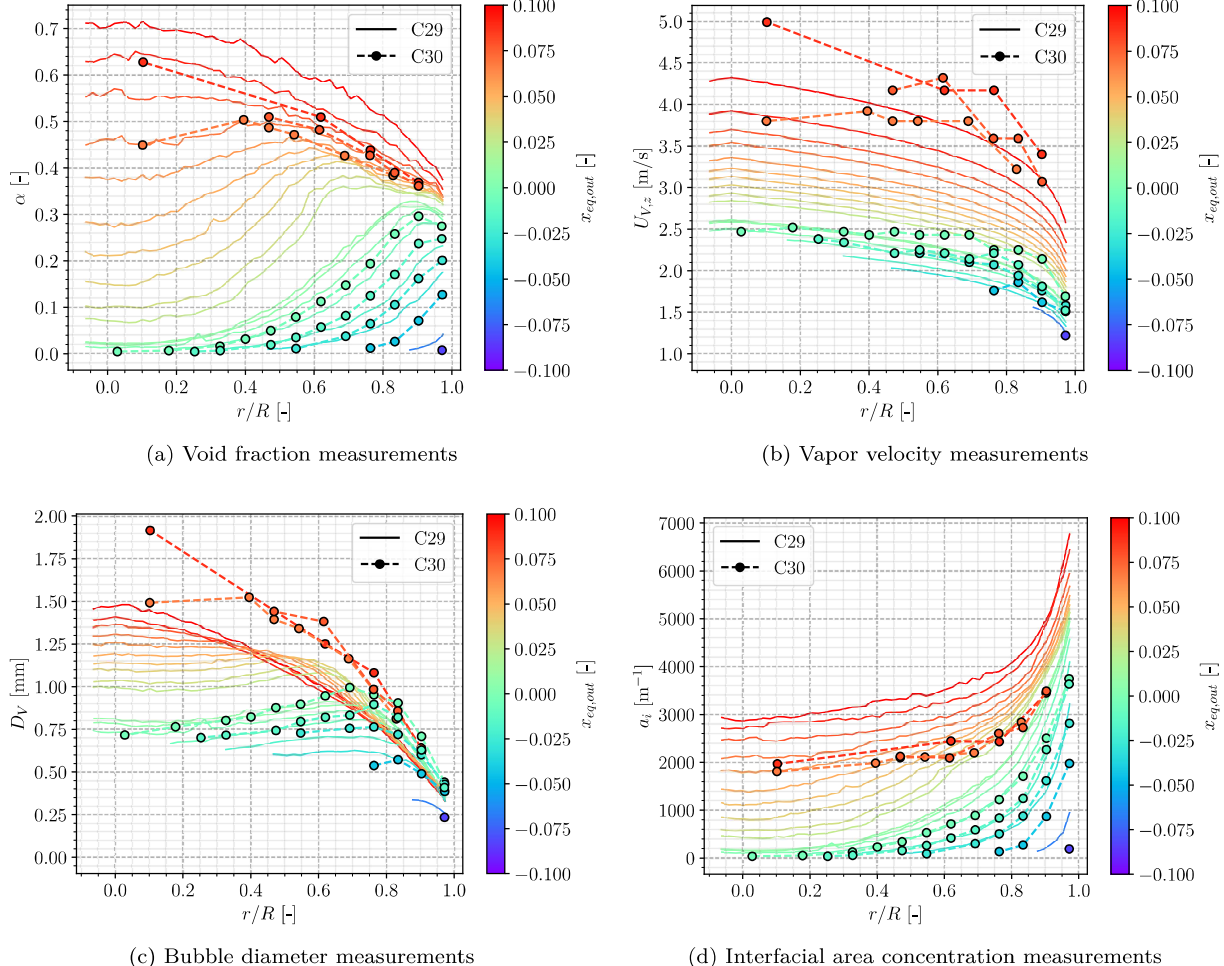


Figure 2.9: 30G2P14W16 and 29G2P14W16 results

Similar to the G2P26W16 cases, we observe the consistency of the void fraction measurements between the C2900 and C300 campaigns (Figure 2.9a). Although the vapor velocity estimation using Eq. 2.8 for C2900 cases also produces acceptable results for subcooled cases, the discrepancy when saturation is reached is even more observed here (Figure 2.9b). The overestimation when $x_{eq,out} > 0$ is larger than for the G2P26W16 cases, with nearly 1 m/s error on hottest cases.

This logically yields larger underestimations of the bubble diameter and associated overestimations of the interfacial area concentration.

The void fraction profiles (Figure 2.9a) present a particular evolution with a moving α peak that shifts from the wall to the bulk as the outlet quality increases. This may indicate a particular bubble dynamics regime inducing transverse bubble migration and accumulation far from the wall. Bulk void fraction can reach values as high as 70% with a flattening profile when $x_{eq,out} \rightarrow 0.1$.

Remark : It seems that saturated cases tend to reach a fixed value of near-wall void fraction between 35% and 40%.

Similar to previous observations, the bubble diameter grows when moving to the bulk, also presenting a peak value around $0.8 > r/R > 0.6$ for subcooled cases (Figure 2.9c). The saturated cases however

present much larger increase in bubble diameter when reaching the bulk flow, with D_V close to 2 mm for the hottest case. This definitely indicates predominant coalescence effects.

Remark : $D_V \approx 2$ mm is observed at a point where $\alpha > 60\%$ which shows that even at such high void fraction values, the flow is still in a bubbly regime with small vapor inclusions ($D_V \approx 0.1D_h$).

The vapor velocity also increases with the outlet quality (Figure 2.9b), but reaches much larger value compared to the G2P26W16 cases. This may be due to the larger bubble size and local void fractions associated to the imposed mass flow rate.

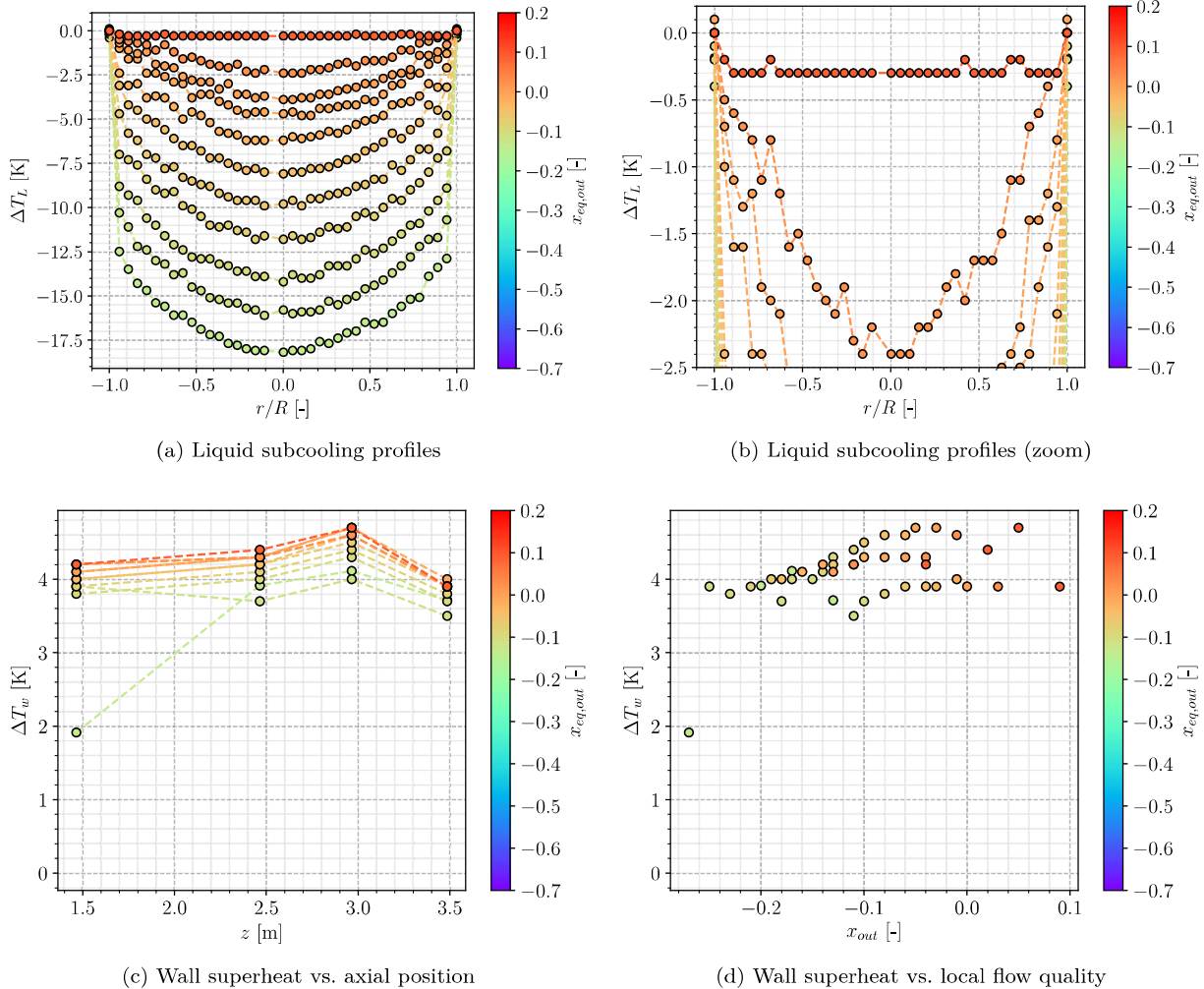


Figure 2.10: 8G2P14W16 results

The liquid temperature profiles (Figure 2.10a) are behaving in a very similar way to the G2P26W16 cases (Figure 2.8a): stable parabolic profile, linear shift with inlet quality and flattening when reaching superheated conditions ($x_{eq,out} \sim 0.1$).

We also have the huge temperature jump when approaching the wall which reduces when reaching boiling regimes. The measurements also detect superheated liquid near the wall for the hottest cases ($\Delta T_L \approx 0.1^\circ$). The case with the greatest outlet quality presents a surprisingly flat liquid temperature profile with measurements being nearly constant ($\Delta T_L = -0.3^\circ\text{C}$) over the whole measurement section.

Remark : Such a constant temperature profile could be interpreted as a limit of the liquid temperature in this regime. Since it corresponds to flow conditions where void fraction is large ($\alpha > 60\%$) and bubbles do not condense (Figure 2.9c), any extra heat input may only contribute to phase change and leave the liquid phase thermally unchanged.

Unfortunately, the 8G2P15W16 campaign did not cover as large quality range as the 8G2P26W16 campaign. We thus do not have access to many single-phase flow wall temperature measurements (Figure 2.10c). Only one point for $x_{eq,out} \approx -0.1$ seem to be in the single-phase convection region. All the other measurements are close to each other and correspond to boiling regimes where we observe a wall superheat stabilization around $\Delta T_w = 4^\circ\text{C}$.

The comparison of wall temperature with local flow quality (Figure 2.10d) is not as interesting as the G2P26W16 cases but still display a welcomed overlapping of the measurements over the different inlet temperatures.

2.5 FURTHER VERIFICATIONS

2.5.1 Reconstruction of the Applied Heat Flux

To further quantify the coherency of the DEBORA database, we want to reconstruct the wall heat flux injected in the flow from the experimental measurements of void fraction, vapor velocity and liquid temperature measurements.

2.5.1.1 Methodology

To do so, we will estimate the total enthalpy change between the inlet and outlet. The inlet liquid enthalpy $h_{L,in}$ is estimated using the inlet temperature and the outlet mixture enthalpy $h_{M,out}$ is computed as:

$$h_{M,out} = x_{m,out} h_{V,sat} + (1 - x_{m,out}) \langle h_{L,out} \rangle_2 \quad (2.13)$$

supposing that the vapor is at saturation temperature and where $x_{m,out}$ is the outlet mass quality.

Using the experimental values of α and $U_{V,z}$, we can compute the outlet mass quality $x_{m,out}$ as:

$$x_{m,out} = \frac{\rho_V \langle \alpha U_{V,z} \rangle_2}{G} \quad (2.14)$$

where:

$$\langle \alpha U_{V,z} \rangle_2 = \frac{1}{\pi R^2} \int_{\vartheta=0}^{2\pi} \int_{r=0}^R \alpha(r) U_{V,z}(r) r dr d\vartheta = \frac{2}{R^2} \int_{r=0}^R \alpha(r) U_{V,z}(r) r dr \quad (2.15)$$

for an axisymmetric profile such as the DEBORA measurements.

From the mass quality we can compute the mixture enthalpy as:

$$h_M = x_m h_{V,sat} + (1 - x_m) \frac{\langle \rho_L (1 - \alpha) U_{L,z} h_L \rangle_2}{\langle \rho_L (1 - \alpha) U_{L,z} \rangle_2} \quad (2.16)$$

Similarly, the average liquid enthalpy at the outlet is estimated as:

$$\langle h_L \rangle_2 = \frac{2}{R^2} \frac{1}{G_L} \int_{r=0}^R \rho_L(r) U_{L,z}(r) h_L(r) r dr \quad (2.17)$$

where h_L is estimated using the local temperature measurements and $U_{L,z}$ is estimated using the drift velocity of Ishii [28]:

$$U_{L,z} = U_{V,z} - U_{rel} = U_{V,z} - \sqrt{2} \left(\frac{g\sigma(\rho_L - \rho_V)}{\rho_L^2} \right)^{1/4} (1 - \langle \alpha \rangle_2)^{1.75} \quad (2.18)$$

Then, writing the one-dimensional energy balance of the flow permits to express the actually applied heat flux:

$$G\pi R^2 (h_{M,out} - h_{L,in}) = \Phi_w = \phi_w 2\pi R L_{heat} \Rightarrow \phi_w = \frac{(h_{M,out} - h_{L,in}) GR}{2L_{heat}} \quad (2.19)$$

which can be compared to the given control parameter for the experiment.

2.5.1.2 Application

To apply the presented reconstruction of the heat flux, we either need:

- A pure single-phase case with an outlet liquid temperature profile (C800 case alone);
- A boiling two-phase case with void fraction and vapor velocity measurements (C3000 case) along with liquid temperature (C800 case).

This means that for boiling cases, we need to "merge" cases from the C3000 and C800 campaign conducted in very close operating conditions (P , G , $T_{L,in}$) and assume that the liquid temperature measurements of the C800 case are actually representative of the liquid temperature in the C3000 case and reciprocally for the void fraction and vapor velocity.

Such a constraint leaves us with very few boiling cases that can accommodate those conditions. They are summed up on Table 2.5.

Case Name	P [bar]	G [kg/m ² /s]	ϕ_w [kW/m ²]	$T_{L,in}$ [°C]	$x_{eq,in}$ [-]	$x_{eq,out}$ [-]
30G2P26W16Te66	26.2	2049.0	73.893	66.59	-0.2919	0.014
8G2P26W16Te66.6	26.2	1982.0	73.9	66.57	-0.2927	0.0237
30G2P26W16Te70	26.19	2051.2	73.893	70.59	-0.2386	0.067
8G2P26W16Te70.3	26.2	1983.0	73.9	70.31	-0.2428	0.0734

Table 2.5: Similar conditions cases between the C3000 and C800 campaigns. Outlet quality calculated with Eq. 2.9.

To actually compute the surface-averaged quantities, we need to interpolate the experimental profiles which is done using the `python` package `scipy`. Figure 2.11 presents typical interpolation profiles used in this sections.

The results obtained for the heat flux recalculations are presented on Table 2.6.

Case name	x_m [-]	$\phi_{w,rec}$ [kW/m ²]	$\phi_{w,exp}$ [kW/m ²]	$\Delta\phi_w$ [%]
30G2P26W23Te66.6	0.0193	70.432	73.893	-4.68%
30G2P26W23Te70.6	0.0500%	68.041	73.893	-7.9%

Table 2.6: Heat flux recalculation results

We see that reconstructing the heat flux yields values significantly lower than the experimental values given in the database. This underestimation was also noted in a similar approach conducted by Guéguen [24] who found discrepancy of a few %.

In our case, these discrepancies can be partially explained by:

- The difference of inlet mass fluxes that are roughly 70 kg/m²/s lower for the C800 cases ;
- The difference of inlet liquid temperature for the Te70 cases with a C800 case 0.3°C lower than the C300 case.

Those small discrepancies lead to outlet qualities (computed with Eq. 2.9 using the given ϕ_w) that differ of approximately 1%. Even though boiling flows near saturation, such as those studied here, are very sensitive to the local quality and flow parameters, this would hardly suffice to explain differences in heat flux as much as 5%.

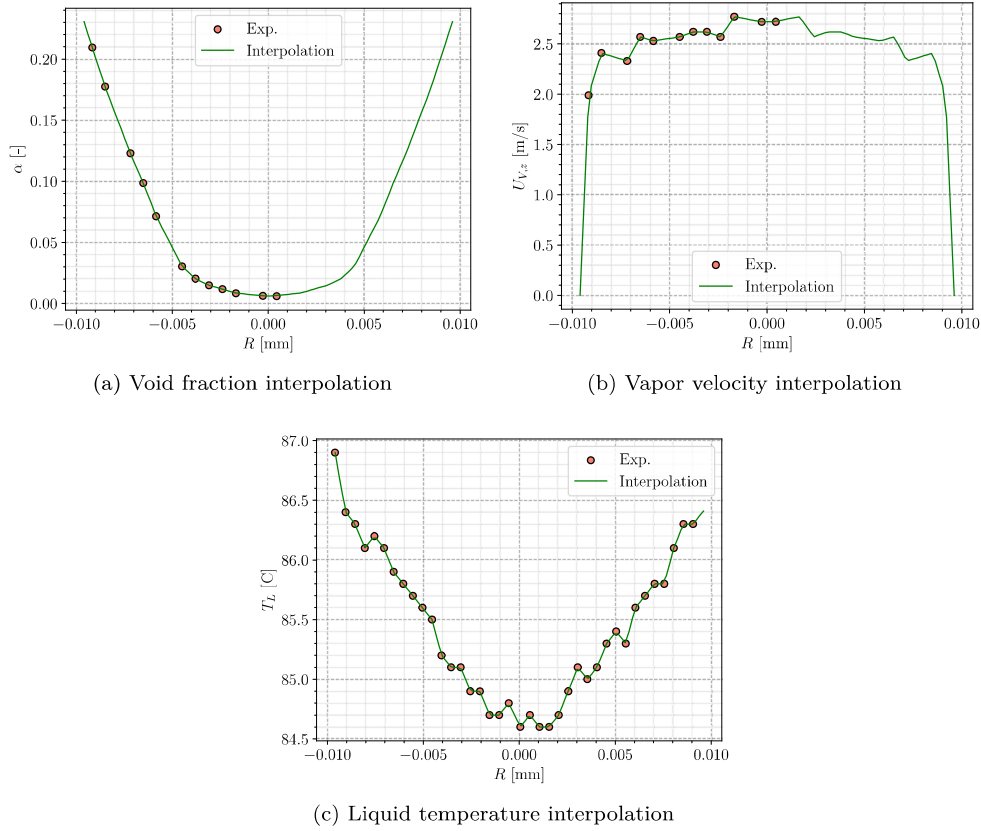


Figure 2.11: Interpolation profiles for cases Te66 (Table 2.5).

Remark : Unfortunately, our methodology do not rely on collocated measurements of all the variables of interest since the campaigns were conducted separately. The "correction" values presented in Table 2.6 can not be considered as accurate estimations but still point out that an uncertainty over the heat flux can be considered in further work.

2.5.2 Verification of Wall Temperature Measurements

In order to test the coherency of wall temperature measurements both in single phase and boiling regions, we compare them to one-dimensional correlations along the $(\Delta T_w, x_{eq})$ curve.

Single-phase measurements are confronted to the estimations of Dittus-Boelter (Eq. 2.20) correlation and Gnielinski correlation (Eq. 2.21):

$$\text{Nu}_{DB} = 0.023 \left(\text{Re}^{4/5} \right) \text{Pr}^{0.4} \quad (2.20)$$

$$\text{Nu}_G = \frac{\frac{C_f}{2} (\text{Re} - 1000) \text{Pr}}{1 + 12.7 \sqrt{\frac{C_f}{2}} \left(\text{Pr}^{2/3} - 1 \right)} \quad (2.21)$$

where the friction coefficient C_f is estimated following Churchill [8] as recommended by Delhayé [13] and Guégan [24]:

$$C_f = 2 \left[\left(\frac{8}{\text{Re}} \right)^{12} + \frac{1}{(A+B)^{1.5}} \right]^{1/12} \quad (2.22)$$

$$A = \left[2.457 \ln \left(\frac{1}{\left(\frac{7}{\text{Re}} \right)^{0.9} + 0.27 \frac{\varepsilon}{D_h} } \right) \right]^{16} \quad (\varepsilon=0 \text{ supposed here})$$

$$B = \left(\frac{37530}{\text{Re}} \right)^{16}$$

Wall superheat in boiling region is compared with the simple correlation of Frost & Dzakowic [20]:

$$\Delta T_{w,FD} = \text{Pr}_{L,sat} \sqrt{\frac{8\sigma\phi_w T_{sat}}{\lambda_{L,sat} h_{LV} \rho_V}} \quad (2.23)$$

where T_{sat} is expressed in Kelvin.

The results are presented on Figure 2.13 for cases at 26 bar and Figure 2.12 for cases at 14 bar. Since we do not need combination with void fraction measurements, every cases of the C800 campaign were used for comparison.

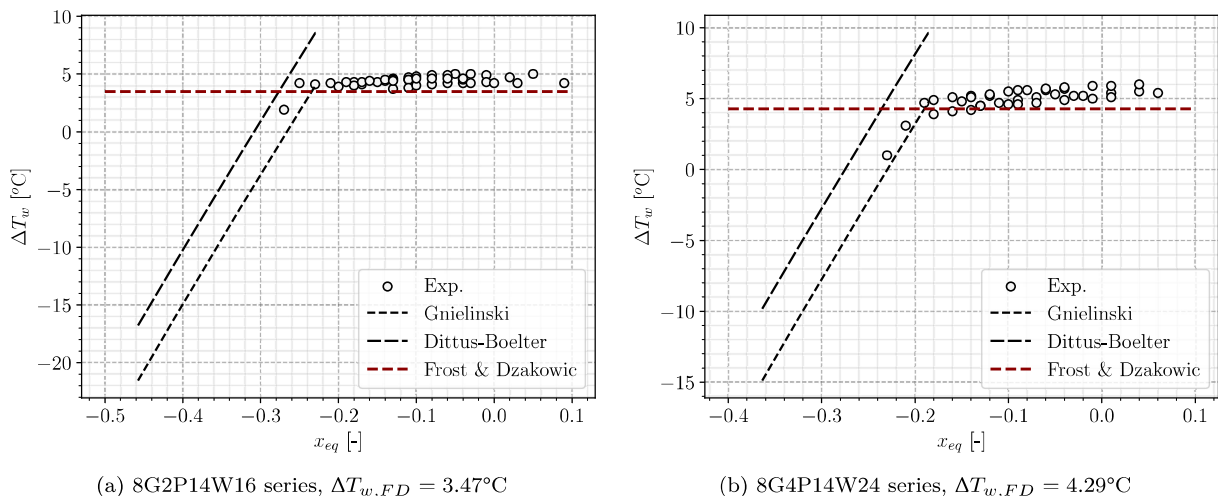


Figure 2.12: Correlations comparison with P14 cases.

Wall temperature measurements for the liquid convective regime are in fairly good agreement with the predictions of the Gnielinski correlation. The slope of the model is very close to the experimental data in the single-phase region. It is particularly true for the P26 cases (Figure 2.13) where a large range of subcooled conditions in the single-phase region was covered.

Regarding the P14 cases (Figure 2.12), very few measurements are available outside of the boiling region. However we can see that the Gnielinski correlation seem to consistently meet the boiling measurements and follow a trend that agrees with the experimental data.

On the other hand, the Dittus-Boelter correlation fails to predict the wall temperature with a constant overestimation of approximately 5°C regardless of the case.

Note : The average liquid temperature at different heights was estimated using a one-dimensional energy balance before computing the local wall temperature predicted by correlations. The virtual length used for single-phase correlations was adjusted to cover the whole range of x_{eq} .

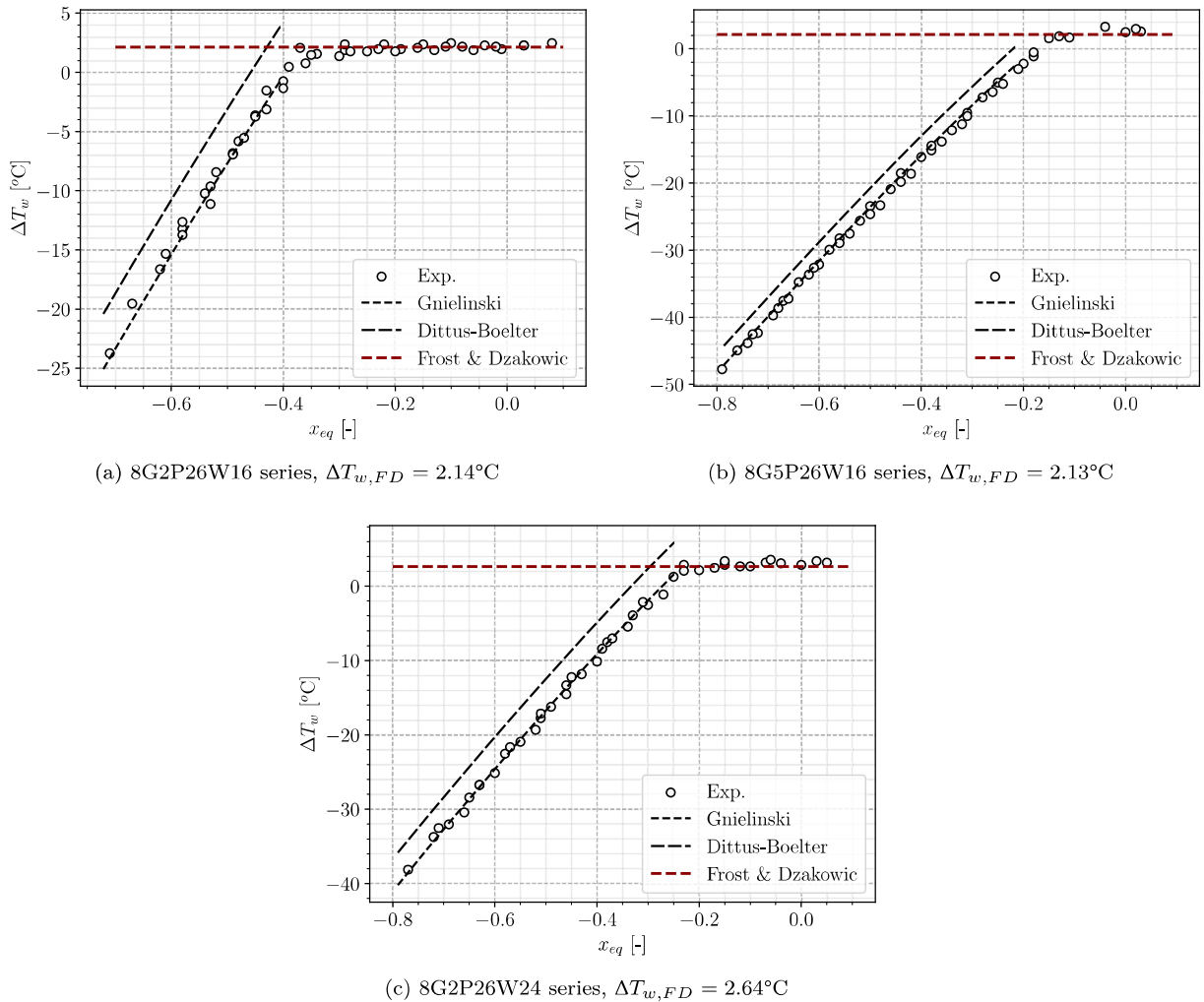


Figure 2.13: Correlations comparison with P26 cases.

The nucleate boiling temperature predicted by Frost & Dzakowic correlation are in good agreement with the experimental observations where we saw the wall temperature stabilization. The prediction is better for the P26 cases than for the P14 cases where an underestimation of 1°C is observed. We can also note that the measurements are more dispersed for the P14 cases and span over a range of more than 1°C around the average temperature.

Those comparisons are comforting the consistency of the wall temperature database which correspond to traditional behavior of wall to fluid heat transfer in both single-phase and boiling two-phase regimes.

2.6 CONCLUSIONS

The DEBORA database is a very rich source of experimental insights for boiling flows representative of PWR industrial conditions. The large range of control parameters that was covered during the tests also is encouraging regarding the variety of flow regimes that can occur in PWR conditions

After a finer analysis of the data, in the continuation of the work of Cubizolles [11], Manon [44] and Guéguen [24], we concluded that:

- The test matrix unfortunately shows that very few series were covered with both bi-optical probe (C3000) and thermocouples (C800) measurements, limiting the availability of a full boiling database to the series G2P26W16 and G2P14W16.
- Small but significant errors on the reported outlet quality could be observed when compared to a one-dimensional energy balance based on the control parameters (Table 2.4).

- Good agreement was found between the void fraction measurements with the mono (C2900) and bi-optical probe (C3000), which comforts the validity of the acquired data in close flow conditions.
- Extension of the C2900 data to estimate bubble diameter and interfacial area concentration using Eq. 2.8 to compute vapor velocity was acceptable in subcooled conditions but showed increasing underestimations in the saturated region (Figures 2.7b and 2.9b).
- Void fraction measurements in the G2P14W16 series showed a particular behavior with a peak value moving from the wall to the bulk as the inlet temperature increases.
- Bubble diameter measurements clearly exhibited coalescence phenomena when leaving the wall with a maximum value reached at $r/R \approx 0.6$ before decreasing under condensation and / or break-up (Figure 2.7c). It was also observed that measurements closest to the wall were nearly constant among a given test series regardless of the inlet temperature.
- Liquid temperature can overcome the saturation temperature for the hottest cases close to the wall ($T_L - T_{sat} \approx 0.1^\circ\text{C}$) and flattens at the bulk with a subcooling roughly around 0.5°C .
- Wall temperature measurements followed a coherent linear profile in the single-phase region before stabilizing when boiling starts, which was further reproduced by comparison with one-dimensional correlations. Measurements were also overlapping each other when plotted versus the local quality, confirming the transposition between change of inlet temperature and axial translation of the measurement section.
- Reconstruction of the applied wall heat flux in the experiments by merging the values from very close C3000 and C800 cases (Table 2.5) suggested that the heat flux values provided in the measurements were too large by 5% to 8%. Such a large difference is surprising and could partially be explained by the small change of operating conditions between C3000 and C800 cases.

At last, the different evaluations conducted over the chosen experiments have reasonably validated the consistency and coherency of the measurements. Further comparisons with NEPTUNE_CFD simulations will be conducted using the experimental results of the G2P26W16 series. **Still, we keep in mind that an error of a few % is possible on ϕ_w .**

BIBLIOGRAPHY

- [1] T. R. Auton. "The lift force on a spherical body in a rotational flow". fr. In: Journal of Fluid Mechanics 183 (Oct. 1987). Publisher: Cambridge University Press, pp. 199–218. ISSN: 1469-7645, 0022-1120. DOI: [10.1017/S002211208700260X](https://doi.org/10.1017/S002211208700260X).
- [2] V. M. Borishanskii, G. I. Bobrovich, and F. P. Minchenko. "Heat transfer from a tube to water and to ethanol in nucleate pool boiling". In: Problems of Heat Transfer and Hydraulics of Two-Phase Media. Elsevier, 1969, pp. 85–106.
- [3] Mattia Bucci, Jacopo Buongiorno, and Matteo Bucci. "The not-so-subtle flaws of the force balance approach to predict the departure of bubbles in boiling heat transfer". In: Physics of Fluids 33.1 (Jan. 2021). Publisher: American Institute of Physics, p. 017110. ISSN: 1070-6631. DOI: [10.1063/5.0036956](https://doi.org/10.1063/5.0036956).
- [4] Lubomír Bureš and Yohei Sato. "On the modelling of the transition between contact-line and microlayer evaporation regimes in nucleate boiling". en. In: Journal of Fluid Mechanics 916 (June 2021). Publisher: Cambridge University Press. ISSN: 0022-1120, 1469-7645. DOI: [10.1017/jfm.2021.204](https://doi.org/10.1017/jfm.2021.204).
- [5] Deqi Chen, Liang-ming Pan, and Song Ren. "Prediction of bubble detachment diameter in flow boiling based on force analysis". en. In: Nuclear Engineering and Design 243 (Feb. 2012), pp. 263–271. ISSN: 0029-5493. DOI: [10.1016/j.nucengdes.2011.11.022](https://doi.org/10.1016/j.nucengdes.2011.11.022).
- [6] Zhihao Chen, Atsushi Haginiwa, and Yoshio Utaka. "Detailed structure of microlayer in nucleate pool boiling for water measured by laser interferometric method". en. In: International Journal of Heat and Mass Transfer 108 (May 2017), pp. 1285–1291. ISSN: 0017-9310. DOI: [10.1016/j.ijheatmasstransfer.2017.01.003](https://doi.org/10.1016/j.ijheatmasstransfer.2017.01.003).
- [7] Zhihao Chen, Xiaocheng Hu, Kang Hu, Yoshio Utaka, and Shoji Mori. "Measurement of the micro-layer characteristics in the whole range of nucleate boiling for water by laser interferometry". en. In: International Journal of Heat and Mass Transfer 146 (Jan. 2020), p. 118856. ISSN: 0017-9310. DOI: [10.1016/j.ijheatmasstransfer.2019.118856](https://doi.org/10.1016/j.ijheatmasstransfer.2019.118856).
- [8] SW Churchill. "Friction Factor Spans All Fluid-Flow Regimes". In: Chemical Engineering 84 (1977), pp. 91–92.
- [9] Marco Colombo and Michael Fairweather. "Prediction of bubble departure in forced convection boiling: A mechanistic model". en. In: International Journal of Heat and Mass Transfer 85 (June 2015), pp. 135–146. ISSN: 0017-9310. DOI: [10.1016/j.ijheatmasstransfer.2015.01.103](https://doi.org/10.1016/j.ijheatmasstransfer.2015.01.103).
- [10] M. G. Cooper and A. J. P. Lloyd. "The microlayer in nucleate pool boiling". en. In: International Journal of Heat and Mass Transfer 12.8 (Aug. 1969), pp. 895–913. ISSN: 0017-9310. DOI: [10.1016/0017-9310\(69\)90154-9](https://doi.org/10.1016/0017-9310(69)90154-9).
- [11] Géraud Cubizolles. "Etude stéréologique de la topologie des écoulements diphasiques à haute pression". These de doctorat. Ecully, Ecole centrale de Lyon, Jan. 1996.
- [12] Victor H. Del Valle and D. B. R. Kenning. "Subcooled flow boiling at high heat flux". en. In: International Journal of Heat and Mass Transfer 28.10 (Oct. 1985), pp. 1907–1920. ISSN: 0017-9310. DOI: [10.1016/0017-9310\(85\)90213-3](https://doi.org/10.1016/0017-9310(85)90213-3).
- [13] Jean-Marc Delhayé. Thermohydraulique des réacteurs. fr. Google-Books-ID: v8vL04U7Zt4C. EDP Sciences, Dec. 2012. ISBN: 978-2-7598-0308-8.
- [14] Etienne Demarly. "A new approach to predicting departure from Nucleate Boiling (DNB) from direct representation of boiling heat transfer physics". eng. Accepted: 2021-02-19T20:35:27Z ISBN: 9781237640528. Thesis. Massachusetts Institute of Technology, 2020.
- [15] G. Duhar, G. Riboux, and C. Colin. "Vapour bubble growth and detachment at the wall of shear flow". en. In: Heat and Mass Transfer 45.7 (May 2009), pp. 847–855. ISSN: 1432-1181. DOI: [10.1007/s00231-007-0287-y](https://doi.org/10.1007/s00231-007-0287-y).
- [16] Géraldine Duhar. "Croissance et détachement de bulles en paroi d'un écoulement cisaillé : étude expérimentale de l'injection et de l'ébullition nucléée". These de doctorat. Toulouse, INPT, Jan. 2003.

- [17] Géraldine Duhar and Catherine Colin. "Dynamics of bubble growth and detachment in a viscous shear flow". In: *Physics of Fluids* 18.7 (July 2006). Publisher: American Institute of Physics, p. 077101. ISSN: 1070-6631. DOI: [10.1063/1.2213638](https://doi.org/10.1063/1.2213638).
- [18] Carlos E. Estrada-Pérez, Yassin A. Hassan, Bandar Alkhudhiri, and Junsoo Yoo. "Time-resolved measurements of liquid–vapor thermal interactions throughout the full life-cycle of sliding bubbles at subcooled flow boiling conditions". en. In: *International Journal of Multiphase Flow* 99 (Feb. 2018), pp. 94–110. ISSN: 0301-9322. DOI: [10.1016/j.ijmultiphaseflow.2017.10.002](https://doi.org/10.1016/j.ijmultiphaseflow.2017.10.002).
- [19] H. K. Forster and N. Zuber. "Growth of a Vapor Bubble in a Superheated Liquid". In: *Journal of Applied Physics* 25.4 (Apr. 1954). Publisher: American Institute of Physics, pp. 474–478. ISSN: 0021-8979. DOI: [10.1063/1.1721664](https://doi.org/10.1063/1.1721664).
- [20] W Frost, G. S Dzakowic, and American Society of Mechanical Engineers. *An extension of the method for predicting* English. OCLC: 459788171. New York, N.Y.: ASME, 1967.
- [21] J. Garnier, E. Manon, and G. Cubizolles. "LOCAL MEASUREMENTS ON FLOW BOILING OF REFRIGERANT 12 IN A VERTICAL TUBE". English. In: *Multiphase Science and Technology* 13.1&2 (2001). Publisher: Begell House Inc. ISSN: 0276-1459, 1943-6181. DOI: [10.1615/MultScienTechn.v13.i1-2.10](https://doi.org/10.1615/MultScienTechn.v13.i1-2.10).
- [22] C. W. M. van der Geld. "The dynamics of a boiling bubble before and after detachment". en. In: *Heat and Mass Transfer* 45.7 (May 2009), pp. 831–846. ISSN: 1432-1181. DOI: [10.1007/s00231-007-0254-7](https://doi.org/10.1007/s00231-007-0254-7).
- [23] Peng Guan, Li Jia, Liaoifei Yin, and Zetao Tan. "Bubble departure size in flow boiling". en. In: *Heat and Mass Transfer* 51.7 (July 2015), pp. 921–930. ISSN: 1432-1181. DOI: [10.1007/s00231-014-1461-7](https://doi.org/10.1007/s00231-014-1461-7).
- [24] Jil Gueguen. "Contribution à la modélisation multidimensionnelle des écoulements bouillants convectifs en conduite haute pression pour l'application au cas des réacteurs à eau pressurisée". These de doctorat. Grenoble, Dec. 2013.
- [25] Alexandre Guion, Shahriar Afkhami, Stéphane Zaleski, and Jacopo Buongiorno. "Simulations of microlayer formation in nucleate boiling". en. In: *International Journal of Heat and Mass Transfer* 127 (Dec. 2018), pp. 1271–1284. ISSN: 0017-9310. DOI: [10.1016/j.ijheatmasstransfer.2018.06.041](https://doi.org/10.1016/j.ijheatmasstransfer.2018.06.041).
- [26] J. S. Hadamard. "Mouvement permanent lent d'une sphère liquide et visqueuse dans un liquide visqueux". In: *Comptes Rendus Hebdomadaires des Séances de l'Académie des Sciences* 155 (1911), pp. 1735–1738.
- [27] Takashi Hibiki and Mamoru Ishii. "Active nucleation site density in boiling systems". en. In: *International Journal of Heat and Mass Transfer* 46.14 (July 2003), pp. 2587–2601. ISSN: 0017-9310. DOI: [10.1016/S0017-9310\(03\)00031-0](https://doi.org/10.1016/S0017-9310(03)00031-0).
- [28] M. Ishii. *One-dimensional drift-flux model and constitutive equations for relative motion between phases in various* English. Tech. rep. ANL-77-47. Argonne National Lab., Ill. (USA), Oct. 1977. DOI: [10.2172/6871478](https://doi.org/10.2172/6871478).
- [29] B. A Kader and A. M Yaglom. "Heat and mass transfer laws for fully turbulent wall flows". en. In: *International Journal of Heat and Mass Transfer* 15.12 (Dec. 1972), pp. 2329–2351. ISSN: 0017-9310. DOI: [10.1016/0017-9310\(72\)90131-7](https://doi.org/10.1016/0017-9310(72)90131-7).
- [30] Satish G. Kandlikar and Mark E. Steinke. "Contact angles and interface behavior during rapid evaporation of liquid on a heated surface". en. In: *International Journal of Heat and Mass Transfer* 45.18 (Aug. 2002), pp. 3771–3780. ISSN: 0017-9310. DOI: [10.1016/S0017-9310\(02\)00090-X](https://doi.org/10.1016/S0017-9310(02)00090-X).
- [31] J. F. Klausner, R. Mei, D. M. Bernhard, and L. Z. Zeng. "Vapor bubble departure in forced convection boiling". en. In: *International Journal of Heat and Mass Transfer* 36.3 (Feb. 1993), pp. 651–662. ISSN: 0017-9310. DOI: [10.1016/0017-9310\(93\)80041-R](https://doi.org/10.1016/0017-9310(93)80041-R).
- [32] G. Kocamustafaogullari. "Pressure dependence of bubble departure diameter for water". en. In: *International Communications in Heat and Mass Transfer* 10.6 (Nov. 1983), pp. 501–509. ISSN: 0735-1933. DOI: [10.1016/0735-1933\(83\)90057-X](https://doi.org/10.1016/0735-1933(83)90057-X).
- [33] L. D. Koffman and M. S. Plesset. "Experimental Observations of the Microlayer in Vapor Bubble Growth on a Heated Solid". In: *Journal of Heat Transfer* 105.3 (Aug. 1983), pp. 625–632. ISSN: 0022-1481. DOI: [10.1115/1.3245631](https://doi.org/10.1115/1.3245631).

- [34] Ravikishore Kommajosyula. "Development and assessment of a physics-based model for subcooled flow boiling with application to CFD". eng. Accepted: 2021-01-05T23:15:30Z. Thesis. Massachusetts Institute of Technology, 2020.
- [35] Artyom Kossolapov. "Experimental Investigation of Subcooled Flow Boiling and CHF at Prototypical Pressures of Light Water Reactors". PhD Thesis. Massachusetts Institute of Technology, 2021.
- [36] Sir Horace Lamb. Hydrodynamics. en. Google-Books-ID: d_AoAAAAAYAAJ. University Press, 1895. ISBN: 978-1-4086-1332-0.
- [37] Dominique Legendre, Jacques Borée, and Jacques Magnaudet. "Thermal and dynamic evolution of a spherical bubble moving steadily in a superheated or subcooled liquid". In: Physics of Fluids 10.6 (June 1998). Publisher: American Institute of Physics, pp. 1256–1272. ISSN: 1070-6631. DOI: [10.1063/1.869654](https://doi.org/10.1063/1.869654).
- [38] Dominique Legendre and Jacques Magnaudet. "The lift force on a spherical bubble in a viscous linear shear flow". en. In: Journal of Fluid Mechanics 368 (Aug. 1998). Publisher: Cambridge University Press, pp. 81–126. ISSN: 1469-7645, 0022-1120. DOI: [10.1017/S0022112098001621](https://doi.org/10.1017/S0022112098001621).
- [39] M. Lemmert and J.M. Chawla. "Influence of flow velocity on surface boiling heat transfer coefficient". en. In: Heat Transfer in Boiling. Hemisphere. Washington D.C., 1977, pp. 236–246.
- [40] Octave Levenspiel. "Collapse of Steam Bubbles in Water". In: Industrial & Engineering Chemistry 51.6 (June 1959). Publisher: American Chemical Society, pp. 787–790. ISSN: 0019-7866. DOI: [10.1021/ie50594a045](https://doi.org/10.1021/ie50594a045).
- [41] V. G. Levich. Physicochemical hydrodynamics. eng. Prentice-Hall international series in the physical and chemical engineering sciences. OCLC: 1378432. Englewood Cliffs, N.J.: Prentice-Hall, 1962. ISBN: 978-0-13-674440-5.
- [42] J. Magnaudet and I. Eames. "The Motion of High-Reynolds-Number Bubbles in Inhomogeneous Flows". In: Annual Review of Fluid Mechanics 32.1 (2000). _eprint: <https://doi.org/10.1146/annurev.fluid.32.1.659>, pp. 659–708. DOI: [10.1146/annurev.fluid.32.1.659](https://doi.org/10.1146/annurev.fluid.32.1.659).
- [43] Sandipan Maity. "Effect of Velocity and Gravity on Bubble Dynamics". MA thesis. University of California Los Angeles, 2000.
- [44] Etienne Manon. "Contribution à l'analyse et à la modélisation locale des écoulements bouillants sous-saturés dans les conditions des réacteurs à eau sous pression". These de doctorat. Châtenay-Malabry, Ecole centrale de Paris, Jan. 2000.
- [45] Philippe (1970 March. "Caractérisation et modélisation de l'environnement thermohydraulique et chimique des gaines de combustible des réacteurs à eau sous pression en présence d'ébullition". These de doctorat. Aix-Marseille 1, Jan. 1999.
- [46] T. Mazzocco, W. Ambrosini, R. Kommajosyula, and E. Baglietto. "A reassessed model for mechanistic prediction of bubble departure and lift off diameters". en. In: International Journal of Heat and Mass Transfer 117 (Feb. 2018), pp. 119–124. ISSN: 0017-9310. DOI: [10.1016/j.ijheatmasstransfer.2017.09.105](https://doi.org/10.1016/j.ijheatmasstransfer.2017.09.105).
- [47] William H McAdams. Heat transmission. English. OCLC: 683455. New York: McGraw-Hill, 1954.
- [48] Renwei Mei and J. F. Klausner. "Shear lift force on spherical bubbles". en. In: International Journal of Heat and Fluid 15.1 (Feb. 1994), pp. 62–65. ISSN: 0142-727X. DOI: [10.1016/0142-727X\(94\)90031-0](https://doi.org/10.1016/0142-727X(94)90031-0).
- [49] Renwei Mei and James F. Klausner. "Unsteady force on a spherical bubble at finite Reynolds number with small fluctuations in the free-stream velocity". In: Physics of Fluids A: Fluid Dynamics 4.1 (Jan. 1992). Publisher: American Institute of Physics, pp. 63–70. ISSN: 0899-8213. DOI: [10.1063/1.858501](https://doi.org/10.1063/1.858501).
- [50] B. B Mikic, W. M Rohsenow, and P Griffith. "On bubble growth rates". en. In: International Journal of Heat and Mass Transfer 13.4 (Apr. 1970), pp. 657–666. ISSN: 0017-9310. DOI: [10.1016/0017-9310\(70\)90040-2](https://doi.org/10.1016/0017-9310(70)90040-2).
- [51] Louis Melville Milne-Thomson. Theoretical Hydrodynamics. en. Google-Books-ID: A5hRAAAAMAAJ. Macmillan and Company, limited, 1938.

- [52] Tomio Okawa, Tatsuhiro Ishida, Isao Kataoka, and Michitsugu Mori. "Bubble rise characteristics after the departure from a nucleation site in vertical upflow boiling of subcooled water". en. In: Nuclear Engineering and Design. Festschrift Edition Celebrating the 65th Birthday of Prof. Richard T. Lahey, Jr. 235.10 (May 2005), pp. 1149–1161. ISSN: 0029-5493. DOI: [10.1016/j.nucengdes.2005.02.012](https://doi.org/10.1016/j.nucengdes.2005.02.012).
- [53] M. S. Plesset and S. A. Zwick. "The Growth of Vapor Bubbles in Superheated Liquids". en. In: Journal of Applied Physics 25.4 (Apr. 1954). Number: 4, pp. 493–450. ISSN: 0021-8979.
- [54] V Prodanovic, D Fraser, and M Salcudean. "Bubble behavior in subcooled flow boiling of water at low pressures and low flow rates". en. In: International Journal of Multiphase Flow 28.1 (Jan. 2002), pp. 1–19. ISSN: 0301-9322. DOI: [10.1016/S0301-9322\(01\)00058-1](https://doi.org/10.1016/S0301-9322(01)00058-1).
- [55] W. E. Ranz. "Evaporation from drops". In: Chemical Engineering Progress (Jan. 1952). ISSN: 0360-7275.
- [56] Lord Rayleigh. "VIII. On the pressure developed in a liquid during the collapse of a spherical cavity". In: The London, Edinburgh, and Dublin Philosophical Magazine and Journal of Science 34.200 (Aug. 1917). Publisher: Taylor & Francis _eprint: <https://doi.org/10.1080/14786440808635681>, pp. 94–98. ISSN: 1941-5982. DOI: [10.1080/14786440808635681](https://doi.org/10.1080/14786440808635681).
- [57] H. Reichardt. "Vollständige Darstellung der turbulenten Geschwindigkeitsverteilung in glatten Leitungen". In: Zeitschrift Angewandte Mathematik und Mechanik 31 (Jan. 1951). ADS Bibcode: 1951ZaMM...31..208R, pp. 208–219. ISSN: 0044-2267. DOI: [10.1002/zamm.19510310704](https://doi.org/10.1002/zamm.19510310704).
- [58] Tingting Ren, Zhiqiang Zhu, Rui Zhang, Jiangwu Shi, and Changqi Yan. "Development of force balance model for prediction of bubble departure diameter and lift-off diameter in subcooled flow boiling". en. In: International Journal of Heat and Mass Transfer 161 (Nov. 2020), p. 120245. ISSN: 0017-9310. DOI: [10.1016/j.ijheatmasstransfer.2020.120245](https://doi.org/10.1016/j.ijheatmasstransfer.2020.120245).
- [59] Andrew Richenderfer, Artyom Kossolapov, Jee Hyun Seong, Giacomo Saccone, Etienne Demarly, Ravikishore Kommajosyula, Emilio Baglietto, Jacopo Buongiorno, and Matteo Bucci. "Investigation of subcooled flow boiling and CHF using high-resolution diagnostics". en. In: Experimental Thermal and Fluid Science 99 (Dec. 2018), pp. 35–58. ISSN: 0894-1777. DOI: [10.1016/j.expthermflusci.2018.07.017](https://doi.org/10.1016/j.expthermflusci.2018.07.017).
- [60] E. Ruckenstein. "On mass transfer in the continuous phase from spherical bubbles or drops". en. In: Chemical Engineering Science 19.2 (Feb. 1964), pp. 131–146. ISSN: 0009-2509. DOI: [10.1016/0009-2509\(64\)85117-4](https://doi.org/10.1016/0009-2509(64)85117-4).
- [61] P. G. Saffman. "The lift on a small sphere in a slow shear flow". en. In: Journal of Fluid Mechanics 22.2 (June 1965), pp. 385–400. ISSN: 0022-1120, 1469-7645. DOI: [10.1017/S0022112065000824](https://doi.org/10.1017/S0022112065000824).
- [62] V. Scheiff, F. Bergame, J. Sebilleau, P. Ruyer, and C. Colin. "Experimental study of steady and transient subcooled flow boiling". en. In: International Journal of Heat and Mass Transfer 164 (Jan. 2021), p. 120548. ISSN: 0017-9310. DOI: [10.1016/j.ijheatmasstransfer.2020.120548](https://doi.org/10.1016/j.ijheatmasstransfer.2020.120548).
- [63] Valentin Scheiff. "Etude expérimentale et modélisation du transfert de chaleur de l'ébullition transitoire". These de doctorat. Toulouse, INPT, Dec. 2018.
- [64] L. E. Scriven. "On the dynamics of phase growth". en. In: Chemical Engineering Science 10.1 (Apr. 1959), pp. 1–13. ISSN: 0009-2509. DOI: [10.1016/0009-2509\(59\)80019-1](https://doi.org/10.1016/0009-2509(59)80019-1).
- [65] Pengyu Shi, Roland Rzehak, Dirk Lucas, and Jacques Magnaudet. "Drag and lift forces on a rigid sphere immersed in a wall-bounded linear shear flow". en. In: Physical Review Fluids 6.10 (Oct. 2021). Number: 10 Publisher: American Physical Society, p. 104309. ISSN: 2469-990X.
- [66] Rong Situ, Takashi Hibiki, Mamoru Ishii, and Michitsugu Mori. "Bubble lift-off size in forced convective subcooled boiling flow". en. In: International Journal of Heat and Mass Transfer 48.25 (Dec. 2005), pp. 5536–5548. ISSN: 0017-9310. DOI: [10.1016/j.ijheatmasstransfer.2005.06.031](https://doi.org/10.1016/j.ijheatmasstransfer.2005.06.031).
- [67] Jia-Wen Song and Li-Wu Fan. "Temperature dependence of the contact angle of water: A review of research progress, theoretical understanding, and implications for boiling heat transfer". en. In: Advances in Colloid and Interface Science 288 (Feb. 2021), p. 102339. ISSN: 0001-8686. DOI: [10.1016/j.jcis.2020.102339](https://doi.org/10.1016/j.jcis.2020.102339).
- [68] R. Sugrue and J. Buongiorno. "A modified force-balance model for prediction of bubble departure diameter in subcooled flow boiling". en. In: Nuclear Engineering and Design 305 (Aug. 2016), pp. 717–722. ISSN: 0029-5493. DOI: [10.1016/j.nucengdes.2016.04.017](https://doi.org/10.1016/j.nucengdes.2016.04.017).

- [69] R. Sugrue, J. Buongiorno, and T. McKrell. "An experimental study of bubble departure diameter in subcooled flow boiling including the effects of orientation angle, subcooling, mass flux, heat flux, and pressure". en. In: *Nuclear Engineering and Design*. SI : CFD4NRS-4 279 (Nov. 2014), pp. 182–188. ISSN: 0029-5493. DOI: [10.1016/j.nucengdes.2014.08.009](https://doi.org/10.1016/j.nucengdes.2014.08.009).
- [70] Rosemary M. Sugrue. "The Effects of Orientation Angle, Subcooling, Heat Flux, Mass Flux, and Pressure on Bubble Growth and Detachment in Subcooled Flow Boiling". PhD Thesis. Massachusetts Institute of Technology, 2012.
- [71] G. E. Thorncroft, J. F. Klausner, and R. Mei. "An experimental investigation of bubble growth and detachment in vertical upflow and downflow boiling". en. In: *International Journal of Heat and Mass Transfer* 41.23 (Dec. 1998), pp. 3857–3871. ISSN: 0017-9310. DOI: [10.1016/S0017-9310\(98\)00092-1](https://doi.org/10.1016/S0017-9310(98)00092-1).
- [72] G.E. Thorncroft, J.F. Klausner, and R. Mei. "Bubble forces and detachment models". English. In: *Multiphase Science and Technology* 13.3-4 (2001), pp. 35–76. ISSN: 0276-1459. DOI: [10.1615/multscientechn.v13.i3-4.20](https://doi.org/10.1615/multscientechn.v13.i3-4.20).
- [73] V. I. Tolubinsky and D. M. Kostanchuk. "VAPOUR BUBBLES GROWTH RATE AND HEAT TRANSFER INTENSITY AT SUBCOOLED WATER BOILING". English. In: Begel House Inc., 1970. DOI: [10.1615/IHTC4.250](https://doi.org/10.1615/IHTC4.250).
- [74] A. Urbano, S. Tanguy, and C. Colin. "Direct numerical simulation of nucleate boiling in zero gravity conditions". en. In: *International Journal of Heat and Mass Transfer* 143 (Nov. 2019), p. 118521. ISSN: 0017-9310. DOI: [10.1016/j.ijheatmasstransfer.2019.118521](https://doi.org/10.1016/j.ijheatmasstransfer.2019.118521).
- [75] A. Urbano, S. Tanguy, G. Huber, and C. Colin. "Direct numerical simulation of nucleate boiling in micro-layer regime". en. In: *International Journal of Heat and Mass Transfer* 123 (Aug. 2018), pp. 1128–1137. ISSN: 0017-9310. DOI: [10.1016/j.ijheatmasstransfer.2018.02.104](https://doi.org/10.1016/j.ijheatmasstransfer.2018.02.104).
- [76] W. G. J. Van Helden, C. W. M. Van Der Geld, and P. G. M. Boot. "Forces on bubbles growing and detaching in flow along a vertical wall". en. In: *International Journal of Heat and Mass Transfer* 38.11 (July 1995), pp. 2075–2088. ISSN: 0017-9310. DOI: [10.1016/0017-9310\(94\)00319-Q](https://doi.org/10.1016/0017-9310(94)00319-Q).
- [77] L. Van Wijngaarden and D. J. Jeffrey. "Hydrodynamic interaction between gas bubbles in liquid". en. In: *Journal of Fluid Mechanics* 77.1 (Sept. 1976). Publisher: Cambridge University Press, pp. 27–44. ISSN: 1469-7645, 0022-1120. DOI: [10.1017/S0022112076001110](https://doi.org/10.1017/S0022112076001110).
- [78] Junsoo Yoo, Carlos E. Estrada-Perez, and Yassin A. Hassan. "Experimental study on bubble dynamics and wall heat transfer arising from a single nucleation site at subcooled flow boiling conditions – Part 1: Experimental methods and data quality verification". en. In: *International Journal of Multiphase Flow* 84 (Sept. 2016), pp. 315–324. ISSN: 0301-9322. DOI: [10.1016/j.ijmultiphaseflow.2016.04.018](https://doi.org/10.1016/j.ijmultiphaseflow.2016.04.018).
- [79] Junsoo Yoo, Carlos E. Estrada-Perez, and Yassin A. Hassan. "Experimental study on bubble dynamics and wall heat transfer arising from a single nucleation site at subcooled flow boiling conditions – Part 2: Data analysis on sliding bubble characteristics and associated wall heat transfer". en. In: *International Journal of Multiphase Flow* 84 (Sept. 2016), pp. 292–314. ISSN: 0301-9322. DOI: [10.1016/j.ijmultiphaseflow.2016.04.019](https://doi.org/10.1016/j.ijmultiphaseflow.2016.04.019).
- [80] Junsoo Yoo, Carlos E. Estrada-Perez, and Yassin A. Hassan. "Development of a mechanistic model for sliding bubbles growth prediction in subcooled boiling flow". en. In: *Applied Thermal Engineering* 138 (June 2018), pp. 657–667. ISSN: 1359-4311. DOI: [10.1016/j.applthermaleng.2018.04.096](https://doi.org/10.1016/j.applthermaleng.2018.04.096).
- [81] Byong-Jo Yun, Andrew Splawski, Simon Lo, and Chul-Hwa Song. "Prediction of a subcooled boiling flow with advanced two-phase flow models". en. In: *Nuclear Engineering and Design*. SI : CFD4NRS-3 253 (Dec. 2012), pp. 351–359. ISSN: 0029-5493. DOI: [10.1016/j.nucengdes.2011.08.067](https://doi.org/10.1016/j.nucengdes.2011.08.067).
- [82] L. Z. Zeng, J. F. Klausner, and R. Mei. "A unified model for the prediction of bubble detachment diameters in boiling systems— I. Pool boiling". en. In: *International Journal of Heat and Mass Transfer* 36.9 (Jan. 1993), pp. 2261–2270. ISSN: 0017-9310. DOI: [10.1016/S0017-9310\(05\)80111-5](https://doi.org/10.1016/S0017-9310(05)80111-5).
- [83] Lanying Zeng, Fady Najjar, S. Balachandar, and Paul Fischer. "Forces on a finite-sized particle located close to a wall in a linear shear flow". In: *Physics of Fluids* 21.3 (Mar. 2009). Publisher: American Institute of Physics, p. 033302. ISSN: 1070-6631. DOI: [10.1063/1.3082232](https://doi.org/10.1063/1.3082232).
- [84] Pei Zhou, Shiyang Hua, Cai Gao, Dongfang Sun, and Ronghua Huang. "A mechanistic model for wall heat flux partitioning based on bubble dynamics during subcooled flow boiling". en. In: *International Journal of Heat and Mass Transfer* 174 (Aug. 2021), p. 121295. ISSN: 0017-9310. DOI: [10.1016/j.ijheatmasstransfer.2021.121295](https://doi.org/10.1016/j.ijheatmasstransfer.2021.121295).

- [85] Pei Zhou, Ronghua Huang, Sheng Huang, Yu Zhang, and Xiaoxuan Rao. "Experimental investigation on active nucleation site density and bubble departure frequency in subcooled flow boiling by using bubble tracking algorithm". en. In: *International Journal of Heat and Mass Transfer* 148 (Feb. 2020), p. 119081. ISSN: 0017-9310. DOI: [10.1016/j.ijheatmasstransfer.2019.119081](https://doi.org/10.1016/j.ijheatmasstransfer.2019.119081).
- [86] Pei Zhou, Ronghua Huang, Sheng Huang, Yu Zhang, and Xiaoxuan Rao. "Experimental investigation on bubble contact diameter and bubble departure diameter in horizontal subcooled flow boiling". en. In: *International Journal of Heat and Mass Transfer* 149 (Mar. 2020), p. 119105. ISSN: 0017-9310. DOI: [10.1016/j.ijheatmasstransfer.2019.119105](https://doi.org/10.1016/j.ijheatmasstransfer.2019.119105).
- [87] Novak Zuber. "The dynamics of vapor bubbles in nonuniform temperature fields". en. In: *International Journal of Heat and Mass Transfer* 2.1 (Mar. 1961), pp. 83–98. ISSN: 0017-9310. DOI: [10.1016/0017-9310\(61\)90016-3](https://doi.org/10.1016/0017-9310(61)90016-3).
- [88] H. C. Ünal. "Maximum bubble diameter, maximum bubble-growth time and bubble-growth rate during the subcooled nucleate flow boiling of water up to 17.7 MN/m²". en. In: *International Journal of Heat and Mass Transfer* 19.6 (June 1976), pp. 643–649. ISSN: 0017-9310. DOI: [10.1016/0017-9310\(76\)90047-8](https://doi.org/10.1016/0017-9310(76)90047-8).